ISSN 0010-5082, Combustion, Explosion, and Shock Waves, 2021, Vol. 57, No. 3, pp. 270–284. © Pleiades Publishing, Ltd., 2021.
Russian Text © S.P. Borisov, A.N. Kudryavtsev, A.A. Shershnev.

Comparison of Detailed Chemical Models of Hydrogen Combustion in Numerical Simulations of Detonation

S. P. Borisov[a], A. N. Kudryavtsev[a,b], and A. A. Shershnev[a]

UDC 536.46

Published in *Fizika Goreniya i Vzryva*, Vol. 57, No. 3, pp. 18–33, May–June, 2021.
Original article submitted March 23, 2020; revision submitted November 19, 2020; accepted for publication December 2, 2020.

Abstract: Four detailed chemical mechanisms used to describe detonation combustion of hydrogen in oxygen are considered. Ignition delays for various temperatures and pressures are found, the Chapman–Jouguet velocity is determined, and the Zel'dovich–von Neumann–Döring solution for different models is obtained. The effect of dilution of the stoichiometric mixture of hydrogen and oxygen by an inert gas is estimated. Direct numerical simulation of detonation wave propagation in a channel is performed. The emergence of instability of the plane wave and formation of a cellular (multifront) structure are studied. The results predicted by different chemical models are analyzed and compared with each other and with available experimental data.

Keywords: ignition delay, instability of a plane detonation wave, detonation cell size, GPU computations.

DOI: 10.1134/S0010508221030023

INTRODUCTION

At the moment, there are many kinetic mechanisms to describe hydrogen combustion in oxygen. Some of them include more than a hundred reactions and several tens of chemical species; others may contain only several tens of reactions and 5–10 species. Two-stage mechanisms, where the induction period and the stage of chemical transformations are distinguished, have become very popular [1, 2]. However, it is not always possible to use these models in practice because of various problem such as determining the constants in a wide range of parameters and quantitative comparisons with experiments.

The choice of the chemical model to be used in numerical simulations of detonation wave (DW) propagation is an important and urgent issue. For example, Bedarev et al. [3, 4] studied various mechanisms for the description of hydrogen combustion in oxygen and noted that detailed mechanisms adequately reproduce the ignition delay and ensure good agreement with experimental data on the DW propagation velocity and (in mixtures strongly diluted by argon) detonation cell size. Nevertheless, the chemical model may significantly affect the computed results: the profiles of gas-dynamic quantities and the parameters of the cellular structure of the detonation wave computed by different models may be noticeably different. The reasons are the difference in the choice of chemical reactions included into the model and in the values of the coefficients determining the rates of these reactions.

In the present paper, we compare four detailed models of chemical kinetics, which describe hydrogen combustion in oxygen. The ignition delays for different initial temperatures and pressures are determined by solving the problem of an explosion in a constant volume. The one-dimensional DW structure

[a] Khristianovich Institute of Theoretical and Applied Mechanics, Siberian Branch, Russian Academy of Sciences, Novosibirsk, 630090 Russia; bsp5@yandex.ru.
[b] Novosibirsk State University, Novosibirsk, 630090 Russia.

[the Zel'dovich–von Neumann–Döring (ZND) solution] is obtained for different chemical models. The influence of nitrogen addition on the ignition delay and one-dimensional DW structure is estimated. Direct numerical simulations of DW propagation in a plane channel filled with hydrogen–oxygen and hydrogen–oxygen–nitrogen mixtures are performed.

1. GOVERNING EQUATIONS

Detonation in a gas mixture can be described by the Euler equations coupled with equations that describe the kinetics of chemical transformations:

$$\frac{\partial \rho Y_i}{\partial t} + \frac{\partial}{\partial x}(\rho u Y_i) + \frac{\partial}{\partial y}(\rho v Y_i) + \frac{\partial}{\partial z}(\rho w Y_i) = W_i \dot{\omega}_i, \quad i = 1, \ldots, N-1. \tag{1}$$

Here t, x, y, and z are the time and the spatial coordinates, respectively, ρ is the density of the mixture, u is its velocity, N is the number of chemical species of the mixture, Y_i is the mass fraction of the ith species, W_i is the molecular weight, and $\dot{\omega}_i$ is the molar rate of production/destruction of the ith species in chemical reactions. The number of independent equations (1) is $N-1$ because the sum of the partial densities of different species is equal to the total density of the mixture.

In the constant-volume explosion problem, the following equations were integrated for determining the ignition delay:

$$\frac{dY_i}{dt} = \frac{W_i \dot{\omega}_i}{\rho}, \quad i = 1, \ldots, N-1, \tag{2}$$

$$\frac{dT}{dt} = -\frac{1}{\rho c_v} \sum_{i=1}^{N} e_i W_i \dot{\omega}_i \tag{3}$$

[$e_i(T)$ is the internal energy of an individual chemical component of the mixture].

The integration was performed with the use of the RADAU5 code [5] with the time step chosen automatically. The ignition delay τ_{ign} was determined as the time period from the computation start to the instant when the highest temperature growth rate was achieved.

The ZND solution can be obtained for the DW with the velocity equal to or greater than the Chapman–Jouguet (CJ) velocity: $D \geqslant D_{\text{CJ}}$; the conditions $D = D_{\text{CJ}}$ and $D > D_{\text{CJ}}$ correspond to the CJ and overdriven detonations, respectively. The CJ velocity was determined using the SDTools software package [6].

After finding the DW velocity, the following system of conservation laws and equations for concentrations of the mixture components written in a coordinate system where the DW is at rest is solved:

$$\frac{d}{dx}(\rho u) = 0 \quad \rightarrow \quad \rho u \equiv m = \text{const}; \tag{4}$$

$$\frac{d}{dx}(\rho u^2 + p) = 0$$

$$\rightarrow \quad \rho u^2 + p = mu + p \equiv F_u = \text{const}; \tag{5}$$

$$\frac{d}{dx}(\rho u H) = 0 \quad \rightarrow \quad \rho u H \equiv F_e = \text{const}, \tag{6}$$

$$H = F_e/m = \text{const};$$

$$\frac{d}{dx}(\rho u Y_i) = W_i \omega_i \ \rightarrow \frac{dY_i}{dx} = \frac{W_i \dot{\omega}_i}{m}, \tag{7}$$

$$i = 1, \ldots, N-1, \ \ Y_N = 1 - \sum_{i=1}^{N-1} Y_i;$$

$$p = \rho \tilde{R} T = \frac{\tilde{R} T m}{u}, \tilde{R} = \sum_{i=1}^{N} Y_i R_i, \ R_i = \frac{R}{W_i}. \tag{8}$$

Here p is the pressure, T is the temperature, R is the universal gas constant, $H \equiv h + u^2/2$ is the total enthalpy of the mixture, and h is the specific enthalpy of the mixture.

Equations (5) and (6) yield

$$u + \tilde{R}\frac{T}{u} = \frac{F_u}{m}, \qquad u^2 = 2(H-h),$$

$$\frac{u^2}{2} + h = \frac{u^2}{2} + \sum_{i=1}^{N} Y_i h_i(T) = H, \tag{9}$$

where h_i is the enthalpy of the corresponding chemical species. Expressing $\tilde{R}T$ from Eq. (9) and eliminating the velocity, we obtain the following equation for the temperature:

$$f(T) \equiv [2(H-h) + \tilde{R}T]^2$$

$$- 2(F_u/m)^2 (H-h) = 0. \tag{10}$$

In calculating the one-dimensional DW structure, Eqs. (7) are integrated numerically. Knowing the concentrations of the mixture components at a new point and, hence, the specific enthalpy of the mixture h, one can solve the nonlinear equation (10) by this or that iterative method and find the temperature; after that, the velocity and all other gas-dynamic quantities are determined. In our computations, we used the fourth-order Runge–Kutta scheme for integrating Eq. (7), and the temperature was obtained using the Newton iterations.

2. DESCRIPTION OF THE CHEMICAL MODELS

In the present paper, we consider four chemical models, which describe hydrogen combustion in oxygen. Each model allows the presence of an inert gas, e.g., nitrogen or argon, as the third species, which does not directly participate in chemical reactions, but affects the reaction rates. The models include up to 20 forward and reverse chemical reactions. The reaction rates are determined from the Arrhenius law

$$k(T) = AT^{\beta} \exp(-E_a/RT). \tag{11}$$

Here the constants A and β, as well as the activation energy E_a are defined by the chemical model. More detailed descriptions of the models under consideration are provided in Appendix.

The simplest model in the study is the ONERA model [7], which was specially developed to describe supersonic combustion. It includes 7 chemical species (H, O, H_2, O_2, OH, H_2O, and N_2) and 7 reactions.

In three other models, there are 9 chemical species: the species used in the ONERA model plus HO_2 and H_2O_2. The Deiterding–Westbrook model described in [8] is an adapted version of the earlier Westbrook model [9], which was developed for detonation in carbon–hydrogen mixtures. The model includes 17 reactions.

The Wilson–MacCormack model [10] is a variation of the Jachimowski model [11] modified to describe supersonic combustion. The model includes 19 reactions, which is greater than that in the previous model by 2.

The last model considered is the Petersen–Hanson model [12], and it should be noted that its was specially developed to take into account the dependence of the chemical reaction rate on pressure. Although this dependence is present only in one reaction, it significantly affects the results. The model includes 20 chemical reactions.

In the first two models, the coefficients are explicitly specified for both forward and reverse reactions. In two other models, the coefficients for the reverse reactions are calculated using the chemical equilibrium constants. Generally speaking, this approach is more correct because it prevents possible inconsistency of the rates of forward and reverse reactions with thermodynamic data. In the present study, the data [13] were used in all cases for calculating the thermodynamic parameters of the mixture components.

3. RESULTS

3.1. Explosion in a Constant Volume

For each chemical model, we calculated the ignition delay τ_{ign} as a function of the initial temperature for stoichiometric mixtures $2H_2 + O_2$ and $2H_2 + O_2 + 3N_2$ for the initial pressures $p_{\text{ini}} = 1$, 10, and 50 atm. The results are shown in Fig. 1.

First of all, it should be noted that the dependence of τ_{ign} on temperature in the ONERA model is much simpler than those in three other models: in fact, it is an exponential dependence for all pressures. Nevertheless, at high temperatures the ONERA model agrees well with the Deiterding–Westbrook and Petersen–Hanson models; at pressures of 1 and 10 atm, the ONERA model is in good agreement with the Wilson–MacCormack model as well. With a further increase in pressure, the ignition delay τ_{ign} in the Wilson–MacCormack model in the high-temperature region decreases more slowly than that in other models. As a result, the value of τ_{ign} at $p_{\text{ini}} = 50$ atm and $T \approx 2000$ K calculated by the Wilson–MacCormack model is higher than the predictions of other models by 4–6 times.

As the temperature decreases, the results predicted by the ONERA model become more and more different from those of other models because of the simplified character of the dependence of τ_{ign} on temperature in this model. In the middle range of temperature ($T \approx 1000$ K), the differences reach three orders of magnitude. The remaining three models demonstrate good qualitative and, to a certain degree, quantitative agreement with each other in this temperature range. With a further decrease in temperature, the Petersen–Hanson model starts to display some differences because it includes a reaction with a pressure-dependent rate. Apparently, if this dependence is taken into account, the results calculated by this model for different values of p_{ini} in the low-temperature range are closer to each other as compared to the data obtained with the use of other chemical mechanisms.

In experimental studies of DW propagation, a certain amount of an inert gas is often added to the mixture to obtain a more regular cellular pattern and ensure more precise measurements of the detonation cell size, which increases due to dilution of the hydrogen–oxygen mixture. To study the influence of dilution of the mixture with an inert gas, we computed the ignition delays in a stoichiometric mixture of hydrogen and oxygen with addition of an identical number of nitrogen moles ($2H_2 + O_2 + 3N_2$).

The dilution of the mixture produces a common effect in all models: addition of nitrogen usually increases the ignition delay (see Fig. 1). However, in the Wilson–MacCormack and Petersen–Hanson models, there are temperature ranges (near the inflection corresponding to the drastic change in the slope of the curve of τ_{ign} as a function of temperature) where the ignition delay in the mixture without nitrogen is longer.

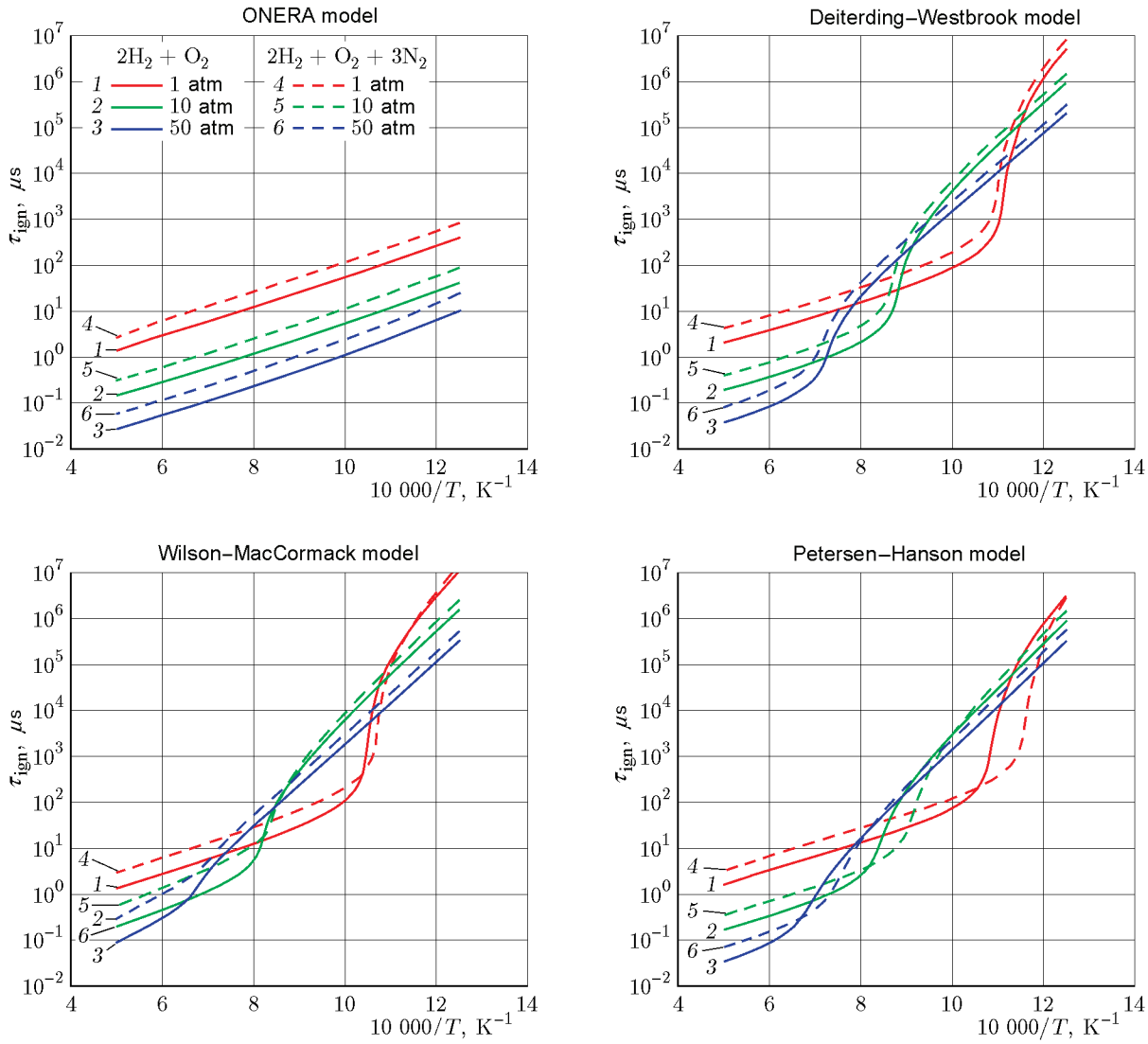

Fig. 1. Ignition delays in the $2H_2 + O_2$ mixture (solid curves) and $2H_2 + O_2 + 3N_2$ mixture (dashed curves) versus temperature calculated by the four models under study.

Thus, the Deiterding–Westbrook, Wilson–MacCormack, and Petersen–Hanson models are in good overall agreement with each other in terms of ignition delay predictions. The ONERA model, which includes a smaller number of chemical species and a significantly reduced set of chemical reactions, yields an essentially different dependence of the ignition delay on temperature, and its predictions at moderate and low temperatures are significantly different from those of other models. However, being specially developed for supersonic flow simulations, this model ensures reasonable results at high temperatures. Simultaneously, in the range of high pressures and high temperatures, i.e., at parameters most typical for detonation combustion, the ONERA model is inconsistent with the Wilson–MacCormack model: the ignition delays predicted by the ONERA model are several times higher.

3.2. Zel'dovich–von Neumann–Döring Solution

The problem of the one-dimensional structure of a plane detonation wave was used for comparisons of the detailed chemical models under study. The first parameter used for comparisons was the detonation propaga-

Table 1. Velocity of detonation wave propagation in the Chapman–Jouguet regime

Chemical model	DW velocity in the mixture [m/s]			
	$2H_2 + O_2$		$2H_2 + O_2 + 3N$	
	$p_{ini} = 1$ atm	$p_{ini} = 0.1$ atm	$p_{ini} = 1$ atm	$p_{ini} = 0.1$ atm
ONERA	2835.19	2710.32	2055.65	1990.87
Deiterding–Westbrook Wilson–MacCormack Petersen–Hanson	2834.97	2710.25	2055.61	1990.86

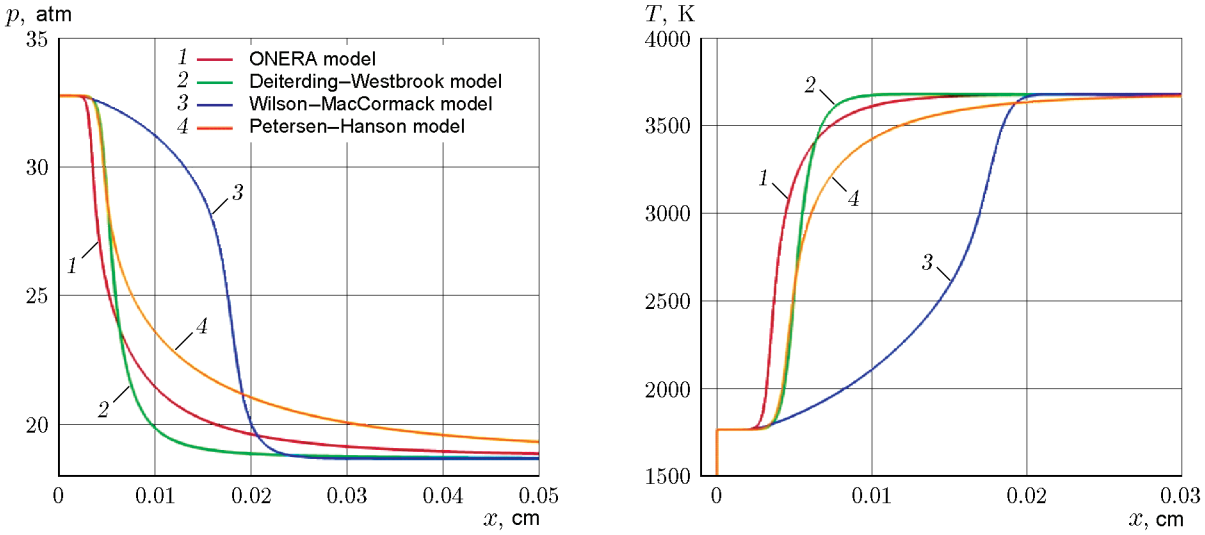

Fig. 2. Pressure and temperature versus the distance in the ZND solution for all models under study. Stoichiometric mixture $2H_2 + O_2$.

tion velocity in the CJ regime D_{CJ}. As mentioned before, it was determined using the SDTools free software [6]. The results are summarized in Table 1.

As is seen from Table 1, it is only the ONERA model that predicts a slightly different CJ velocity; the values obtained by other models agree with high accuracy. It is an expected result because the equilibrium composition of the mixture at the given pressure and temperature corresponds to the minimum value of the thermodynamic Gibbs potential. Thus, for models with an identical set of chemical components, the equilibrium composition at the CJ point and, hence, the velocity are identical if the same dependences of the thermodynamic functions of individual species on temperature are used.

After that, we computed the one-dimensional DW structure (ZND solution) in the case of the CJ detonation for all chemical models and two types of stoichiometric mixtures: hydrogen–oxygen mixture ($2H_2 + O_2$) and hydrogen–oxygen–nitrogen mixture ($2H_2 + O_2 + 3N_2$) with the initial pressure of 1 atm and initial temperature of 300 K. The pressure and temperature are plotted in Fig. 2 as functions of the distance from the shock wave front.

It is seen that the smallest distance between the shock wave front and the point where the combustion process begins is predicted by the ONERA model, whereas the Deiterding–Westbrook and Petersen–Hanson models yield a slightly greater distance. At the beginning, the curves constructed by these two models almost coincide; however, further downstream, the pressure and temperature predicted by the Petersen–Hanson model change more slowly and reach their equilibrium values at a greater distance from the shock wave.

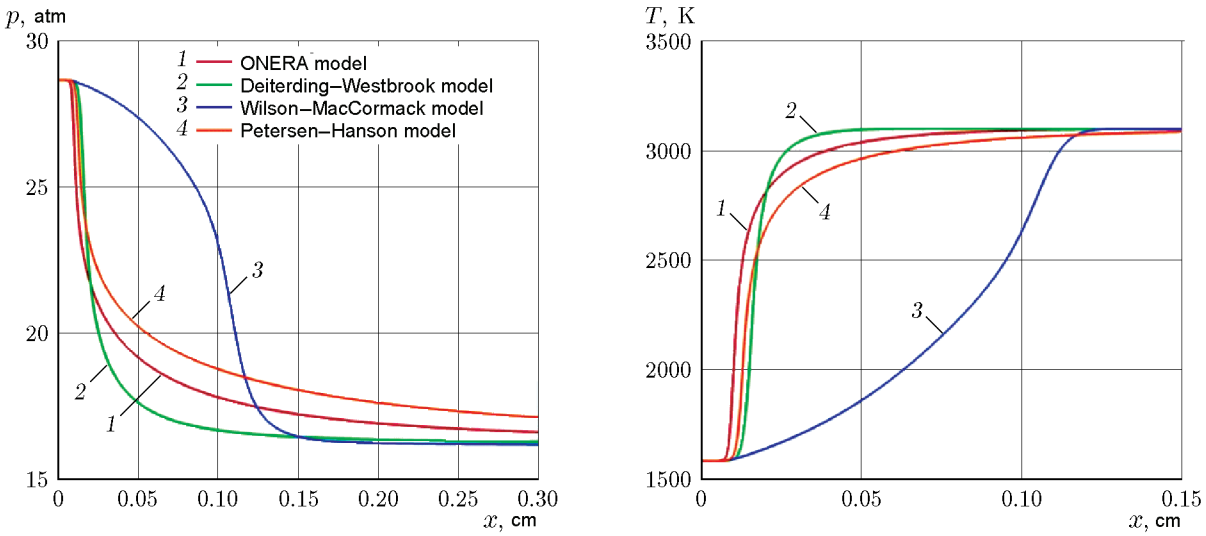

Fig. 3. Pressure and temperature versus the distance in the ZND solution for all models under study. Stoichiometric hydrogen–oxygen mixture diluted by 50% of nitrogen: $2H_2 + O_2 + 3N_2$.

The behaviors of the pressure and temperature profiles in the Wilson–MacCormack model are significantly different. Although the chemical reactions start approximately at the same distance from the shock wave, the combustion region is several times longer and the point with the maximum heat release is located noticeably farther from the shock wave front. This behavior is consistent with the calculated ignition delay in the previous Section. Indeed, the temperature behind the shock wave front is 1769 K, and the pressure is approximately 33 atm. These values correspond to the high-pressure and high-temperature region in Fig. 1, where the ignition delay predicted by this model is several times higher than the values predicted by the other chemical mechanisms.

Addition of 50% of nitrogen to the stoichiometric mixture of hydrogen and oxygen causes significant changes in the DW structure (Fig. 3). The values of the main parameters behind the shock wave become smaller: the pressure decreases from 33 to 29 atm, and the temperature decreases from 1760 to 1590 K. The distance between the wave front and the ignition point significantly increases, and the heat release region proper becomes more extended. The value far downstream (near the CJ point) also change: the pressure decreases from 19 to 16.7 atm, and the temperature decreases from 3680 to 3100 K. We can say that addition of an inert gas makes the detonation less violent, and it occurs at greater scales in space and time.

It should be expected that larger and more regular detonation cells would appear in numerical simulations of propagation of the multifront DW, as it is observed in real physical experiments.

3.3. Direct Numerical Simulation of Detonation Wave Propagation in a Plane Channel

It is well known that the DW front is unstable to transverse perturbations. Two-dimensional direct numerical simulations allow one to study the influence of the chemical model on the evolution of this instability and on the formation of the cellular structure of the detonation wave. Such simulations were performed by the numerical code developed by the authors for solving the Euler equations for a chemically reacting gas [14]. The code involves a third-order TVD scheme for approximation of convective terms and a semi-implicit Runge–Kutta scheme ASIRK-2C for integrating the equations with respect to time. Owing to the use of the semi-implicit scheme, it is possible to attenuate the constraints on the time step, which follow from the stability conditions for stiff chemical source terms. The code is written in the C++ language and is parallelized with the MPI, OpenMP, and CUDA technologies. It allows computations to be performed both on usual multiprocessor and multicore computers and also on computers with a hybrid architecture including graphics processing units (GPUs) or Xeon Phi co-processors.

All computations were performed for the initial temperature of the mixture equal to 300 K. Figure 4 illustrates the onset of instability of the propagating plane wave to transverse perturbations. The figure shows the time evolution of the DW front coordinate obtained in computing the wave propagation in a channel 1 cm wide filled with a stoichiometric hydrogen–oxygen mixture at the initial pressure of 1 atm. The computations were performed with the ONERA and Wilson–MacCormack models for a DW with the overdrive ratio $f = 1.4$ and theoretical velocity $D(f) = D_{\mathrm{CJ}}\sqrt{f}$.

The case with an overdriven DW was chosen to avoid the emergence of one-dimensional fluctuations, which complicate the pattern of instability development. It is well known that overdriven DWs are more stable (see, e.g., [15, 16]). In particular, as can be seen from the one-dimensional computations [17], an increase in the overdrive ratio up to $f = 1.4$ guarantees suppression of instability to streamwise perturbations. Moreover, in the overdriven regime, the oscillations of the front velocity have a more "ordered" character, so that it is easier to trace the changes in the front position with time in one figure.

The ZND solution for the overdriven wave was used as the initial flow field. The computation was performed in a coordinate system moving with the velocity $D(f)$, i.e., in theory, the DW position is unchanged during the computation. The computational domain length was 1.5 cm, which was much greater than the reaction region width. Uniform free-stream conditions were imposed at the inflow boundary, and the parameters corresponding to the equilibrium values far downstream from the DW front were set at the outflow boundary. The computation was performed on a grid with 600 × 400 cells.

As is seen from Fig. 4, after a certain small shift at the very beginning of the computation, the DW front position does remain unchanged for a long time. However, transverse perturbations appear on the wave front afterwards.

Figure 4 shows both the front position near one of the channel walls and the front position averaged over the channel width. Their difference clearly indicates that the leading front of the DW is far from being plane. It should be noted that the DW velocity after the emergence of transverse waves becomes slightly higher than $D(f)$ predicted by the one-dimensional theory; therefore, in the coordinate system used here, it slowly moves in the upstream direction. For the ONERA model, this excess of velocity is approximately 3.25 m/s, which is smaller than 0.1% of the DW propagation velocity.

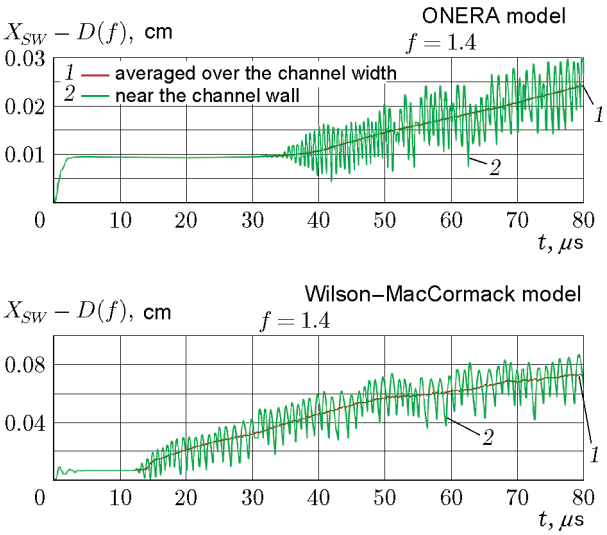

Fig. 4. Time evolution of the DW front averaged over the channel width (curve *1*) and near one of the walls (curve *2*).

In the computation with the Wilson–MacCormack model, the transverse perturbations at the wave front arise noticeably earlier than in the case with the ONERA model. After that, the DW also starts to move upstream, and its velocity is higher than the theoretical velocity by 12.3 m/s. However, the velocity decreases at a certain instant, which is manifested in the lower part of Fig. 4 as an inflection on the corresponding curve at $t \approx 47.5$ μs. Since that instant and up to the end of the computation, the velocity is higher than the value predicted by the one-dimensional theory approximately by 6.15 m/s.

It should be noted that the fact that the multifront DW velocity can be greater than the value calculated in the absence of transverse fluctuations was mentioned back in the classical monographs [18, 19]. Detonation propagation with a velocity slightly higher than the CJ velocity was also observed in physical experiments.

The emergence and growth of transverse waves rapidly lead to the formation of an unsteady two-dimensional cellular structure. The detonation cells are rather small at first, but they merge with time, and their size increases. For the ONERA model, the time instant $t \approx 50$ μs, when large cells start to prevail, corresponds to certain changes in the character of oscillations of the front position (see Fig. 4). For the Wilson–MacCormack model, it coincides with the instant of the DW velocity reduction mentioned above.

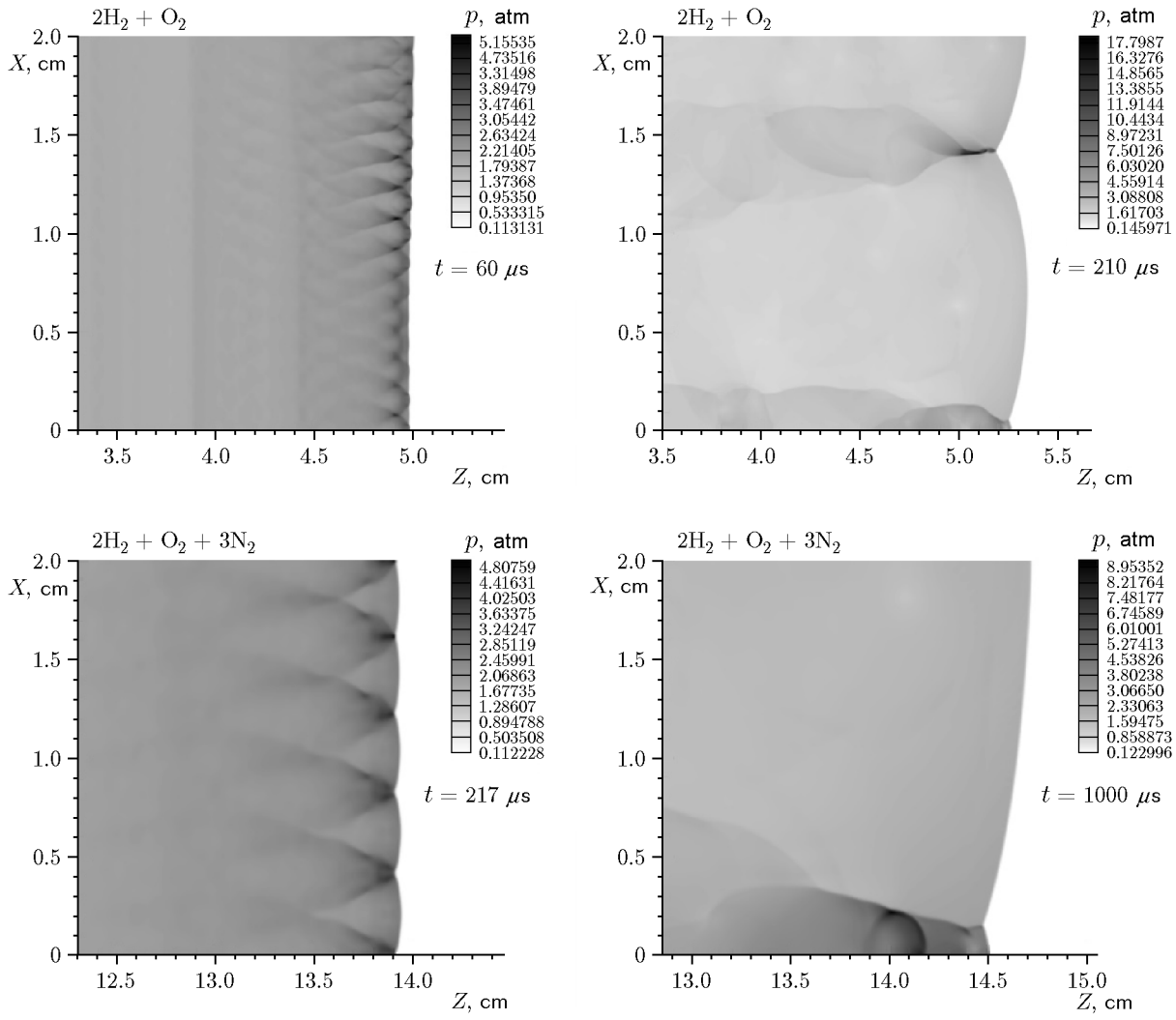

Fig. 5. Linear and nonlinear stages of formation of the cellular DW structure. Petersen–Hanson model ($p_{\text{ini}} = 0.1$ atm and $f = 1$).

Numerical simulations of all stages of the development of the multifront structure were performed for the CJ detonation ($f = 1$) with the use of all four models of chemical kinetics under study for the initial pressure $p_{\text{ini}} = 0.1$ atm. As was mentioned above, the computations were performed for a stoichiometric mixture of hydrogen and oxygen ($2H_2 + O_2$) and for a mixture of hydrogen, oxygen, and nitrogen ($2H_2 + O_2 + 3N_2$). The channel height was 2 cm, and its length was varied in the interval from 6 to 30 cm depending on the model and composition of the mixture. The resolution in each case was chosen to provide 24 computational cells between the shock wave and the point with the maximum heat release. Thus, the final resolution was up to 400 cells in 1 cm and up to 2 000 000 cells in the entire computational domain. Figure 5 shows the pressure fields at different time instants for the two mixtures obtained with the use of the Petersen–Hanson model.

The upper row of Fig. 5 shows typical patterns of multifront detonation in the $2H_2 + O_2$ mixture at two stages of the cellular structure formation. The early, linear, stage at which the growth of instability leads to the formation of numerous small cells is presented on the left. The right part of the figure illustrates the second, essentially nonlinear, stage at which small cells merge until their mean size exceeds the initial size by several times. The lower row shows the same stages for the $2H_2 + O_2 + 3N_2$ mixture. It is clearly seen that the size of the cells being formed depends on the composition of the mixture. If the mixture is diluted

Table 2. Number of detonation cells depending on the model and initial composition of the mixture

Chemical model	Number of detonation cells			
	$2H_2 + O_2$		$2H_2 + O_2 + 3N_2$	
	linear stage	nonlinear	linear stage	nonlinear
ONERA	12.5–13.5	1.5–2	6	0.5
Deiterding–Westbrook	5–6	0.5–v1.5	6.5–9.5	0.5
Wilson–MacCormack	19–21	1–2	6–9.5	0.5
Petersen–Hanson	12–14	1.5	4.5–5	0.5

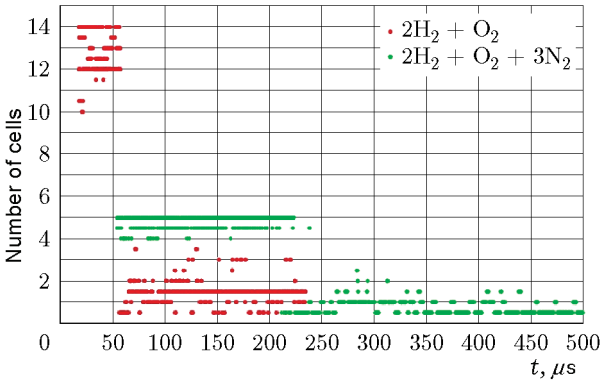

Fig. 6. Number of detonation cells versus time in the computation with the Petersen–Hanson model.

by nitrogen, the cell size increases approximately by a factor of 3: 5 cells emerge at the linear stage instead of 14, which transform to one half-cell at the end of the nonlinear stage, while the non-diluted mixture yields 1.5 cells. As in the case with the ZND solution, the maximum pressure and other parameters are noticeably different as well.

Thus, addition of an inert gas leads to enhancement of the spatial and temperature scales of detonation. This effect has been well known long ago from experiments. This is quantitatively illustrated in Fig. 6, which shows the change in the number of detonation cells with time. The number of cells was calculated by applying the Fourier transform to the DW front shape.

It is clearly seen from Fig. 6 that the cellular structure in the mixture without nitrogen starts to form much earlier ($\approx$15 μs as compared to $\approx$60 μs). The transition to the second stage with a drastic increase in the cell size also occurs earlier.

Dilution with nitrogen exerts an identical qualitative effect on the cellular structure of the DW for all chemical models. The quantitative results are summarized in Table 2. It should be noted that the number and, hence, the size of cells formed at the initial stage of the cellular structure formation depend to a large extent on the model used. It was demonstrated earlier [20–22] that the initial cell size for the simplest chemical model with one irreversible reaction is equal to the wave length of the transverse perturbation, which has the maximum growth rate in accordance with the linear theory of stability. It may be assumed that this statement is also valid for situations with detailed chemical mechanisms. Therefore, the differences observed at the initial stage of the cellular structure formation can be attributed to the differences in the characteristics of stability of the ZND solution for these mechanisms. Unfortunately, it is impossible to verify this assumption because there are no publications that describe computations of linear stability of the DW with detailed chemical models.

The growth and merging of detonation cells at later stages are obviously associated with nonlinear interactions activated when the perturbations reach noticeable amplitudes. The exact mechanism that controls these processes is currently unknown. In computations performed with the simplest model, the size of fully developed detonation cells is approximately twice the cell size at the linear stage [21].

It follows from Table 2 that this feature is not observed in computations with detailed chemical mechanisms. Indeed, despite significant differences in the number of cells at the initial stage, all models yield an approximately identical number of cells at the end of the computation. It should be mentioned, however, that it is desirable to repeat the computations for a wider channel in order to be absolutely sure that this conclusion is valid.

The results of Table 2 can be used to compare the predicted transverse size of fully developed detonation cells with experimental data. The following results were

obtained for the non-diluted stoichiometric mixture of hydrogen and oxygen: 1–13 cm (ONERA model), 1.3–1.4 cm (Deiterding–Westbrook model), 1–2 cm (Wilson–MacCormack model), and 1.3 cm (Petersen–Hanson model). The experimental data [23] for the same parameters yield the cell size of 1.5–1.6 cm.

For the stoichiometric hydrogen–oxygen mixture diluted with nitrogen, all models predict the same detonation cell size: 4 cm. We could not find experimental data for such parameters. However, with extrapolation of data for the closest conditions available [24], the detonation cell size at the pressure of 0.1 atm can be expected to be 5–8 cm, which is also fairly close to the computed values.

CONCLUSIONS

Four models of hydrogen combustion in oxygen were compared. The computation of the ignition delay showed that the dependence of the ignition delay on temperature in the ONERA model has a much simpler, exponential, character as compared to other models. Nevertheless, these differences are manifested to the major extent at moderate and low temperatures, whereas the ignition delays predicted by this model agree well with the data obtained by the Deiterding–Westbrook and Petersen–Hanson models. At the same time, the Wilson–MacCormack model predicts severalfold higher ignition delays in the range of high temperatures and high pressures (most typical for detonation combustion), which differ from the results of other models.

The differences are also observed in computations of the one-dimensional DW structure. For the initial pressure of 1 atm, the distance from the wave front to the point of ignition and the combustion region length computed with the Wilson–MacCormack model are much greater than the corresponding values predicted by other models.

Dilution of the mixture with inert nitrogen produced a qualitatively identical effect for all models. Addition of nitrogen resulted in an increase in the ignition delay and made the detonation less violent by reducing the maximum pressure and temperature behind the DW front and extending the profile of the ZND solution in space. Despite the presence of a pressure-dependent reaction in the Petersen–Hanson model, the results predicted by this model do not differ much from those of other models.

All the models under consideration were verified by their authors with the use of more detailed models, which, in turn, were designed so that they ensured a consistent description of available experimental data. However, the computations show that the models predict different values of parameters in some ranges of temperature and pressure, even of such a basic parameter as the ignition delay. It also seems that the Wilson–MacCormack model is not able to provide an accurate description of detonation combustion at initial pressures close to the atmospheric value. Nevertheless, this model has been often used recently for modeling one-dimensional pulsed instability [25–27].

Direct numerical simulations of DW propagation in a channel performed with different models revealed significant differences in the sizes of detonation cells formed at the initial, linear, stage of the cellular structure formation. It can be assumed that the reason is the differences in the characteristics of linear stability of the ZND solution in situations with different models, namely, different wave length of transverse perturbations with the maximum growth rate. Unfortunately, the available computations of stability characteristics are confined to the simplest model with one irreversible reaction. There are no computations with detailed models, apparently, because the corresponding linearized equations are too cumbersome.

The sizes of fully developed detonation cells formed at the second, nonlinear, stage of the cellular structure formation are in good agreement with each other (in computations with different models) and with available experimental data. However, it should be noted that more precise comparisons require computations in significantly wider channels accommodating a large number of detonation cells because the cell size in narrow channels may significantly change and adapt to the channel width so that the channel could accommodate an integer number of half-cells.

The earliest stages of the formation of a cellular structure from an initially plane DW are demonstrated in more detail by an example of propagation of an overdriven DW. It is shown that the multifront structure starts to form as a result of gradual growth of small transverse perturbations, which most probably appear in computations due to accumulation of rounding errors. It was found that the mean velocity of the DW after the cellular structure formation is slightly higher than the velocity predicted by the one-dimensional theory. This observation is consistent with experimental data.

This work was supported by the Russian Foundation for Basic Research (Grant Nos. 16-57-48007, 18-08-01442, and 18-33-00740).

APPENDIX

ONERA Model

ELEMENTS
H O N
SPECIES
H O H_2 O_2 OH H_2O N_2

No.	Reaction	A, mol, cm^3, s	β	E_a/R, K
1	$H_2 + O_2 \rightarrow 2OH$	$1.700 \cdot 10^{13}$	0	24 043.8
	$H_2 + O_2 \leftarrow 2OH$	$4.032 \cdot 10^{10}$	0.3168	14 553.8
2	$H + O_2 \rightarrow OH + O$	$1.987 \cdot 10^{14}$	0	8455.6
	$H + O_2 \leftarrow OH + O$	$8.930 \cdot 10^{11}$	0.3383	−117
3	$H_2 + OH \rightarrow H_2O + H$	$1.024 \cdot 10^{08}$	1.6	1659.8
	$H_2 + OH \leftarrow H_2O + H$	$7.964 \cdot 10^{08}$	1.528	9300
4	$H_2 + O \rightarrow OH + H$	$5.119 \cdot 10^{04}$	2.67	3163.3
	$H_2 + O \leftarrow OH + H$	$2.701 \cdot 10^{04}$	2.649	2239.6
5	$2OH \rightarrow H_2O + O$	$1.506 \cdot 10^{09}$	1.14	49.8
	$2OH \leftarrow H_2O + O$	$2.22 \cdot 10^{10}$	1.089	8613.2
6	$H + OH + M \rightarrow H_2O + M$	$2.212 \cdot 10^{22}$	−2.0	0
	$H + OH + M \leftarrow H_2O + M$	$8.936 \cdot 10^{22}$	−1.835	59 742.6
	$H_2O/6.5/O_2/0.4/N_2/1.0/$			
7	$2H + M \rightarrow H_2 + M$	$9.791 \cdot 10^{16}$	−0.6	0
	$2H + M \leftarrow H_2 + M$	$5.086 \cdot 10^{16}$	−0.3624	52 104.9
	$H_2/2.5/H_2O/12.0/N_2/1.0/$			

Deiterding–Westbrook Model

ELEMENTS
H O N
SPECIES
H O H_2 O_2 OH H_2O HO_2 H_2O_2 N_2

No.	Reaction	A, mol, cm^3, s	β	E_a, cal/mol
1	$H + O_2 \rightarrow O + OH$	$1.86 \cdot 10^{14}$	0	16 790
	$H + O_2 \leftarrow O + OH$	$1.48 \cdot 10^{13}$	0	680
2	$H_2 + O \rightarrow H + OH$	$1.82 \cdot 10^{10}$	1.0	8900
	$H_2 + O \leftarrow H + OH$	$8.32 \cdot 10^{09}$	1.0	6950
3	$H_2O + O \rightarrow 2OH$	$3.39 \cdot 10^{13}$	0	18 350
	$H_2O + O \leftarrow 2OH$	$3.16 \cdot 10^{12}$	0	1100
4	$H_2O + H \rightarrow H_2 + OH$	$9.55 \cdot 10^{13}$	0	20 300
	$H_2O + H \leftarrow H_2 + OH$	$2.19 \cdot 10^{13}$	0	5150

Deiterding–Westbrook Model (continued)

No.	Reaction	A, mol, cm^3, s	β	E_a, cal/mol
5	$H_2O_2 + OH \rightarrow H_2O + HO_2$	$1.00 \cdot 10^{13}$	0	1800
	$H_2O_2 + OH \leftarrow H_2O + HO_2$	$2.82 \cdot 10^{13}$	0	32 790
6	$HO_2 + O \rightarrow OH + O_2$	$5.01 \cdot 10^{13}$	0	1000
	$HO_2 + O \leftarrow OH + O_2$	$6.46 \cdot 10^{13}$	0	56 160
7	$HO_2 + H \rightarrow 2OH$	$2.51 \cdot 10^{14}$	0	1900
	$HO_2 + H \leftarrow 2OH$	$1.20 \cdot 10^{13}$	0	40 100
8	$HO_2 + H \rightarrow H_2 + O_2$	$2.51 \cdot 10^{13}$	0	700
	$HO_2 + H \leftarrow H_2 + O_2$	$5.50 \cdot 10^{13}$	0	57 800
9	$HO_2 + OH \rightarrow H_2O + O_2$	$5.01 \cdot 10^{13}$	0	1000
	$HO_2 + OH \leftarrow H_2O + O_2$	$6.31 \cdot 10^{14}$	0	73 860
10	$H_2O_2 + O_2 \rightarrow 2HO_2$	$3.98 \cdot 10^{13}$	0	42 640
	$H_2O_2 + O_2 \leftarrow 2HO_2$	$1.00 \cdot 10^{13}$	0	1000
11	$H_2O_2 + H \rightarrow HO_2 + H_2$	$1.70 \cdot 10^{12}$	0	3750
	$H_2O_2 + H \leftarrow HO_2 + H_2$	$7.24 \cdot 10^{11}$	0	18 700
12	$H_2O + M \rightarrow H + OH + M$	$2.19 \cdot 10^{16}$	0	105 000
	$H_2O + M \leftarrow H + OH + M$	$1.41 \cdot 10^{23}$	-2.0	0
	$H_2O/6.5/O_2/0.4/N_2/1.0/$			
13	$H + O_2 + M \rightarrow HO_2 + M$	$1.66 \cdot 10^{15}$	0	-1000
	$H + O_2 + M \leftarrow HO_2 + M$	$2.29 \cdot 10^{15}$	0	45 900
	$H_2O/6.5/O_2/0.4/N_2/1.0/$			
14	$H_2O_2 + M \rightarrow 2OH + M$	$1.20 \cdot 10^{17}$	0	45 500
	$H_2O_2 + M \leftarrow 2OH + M$	$9.12 \cdot 10^{14}$	0	-5070
	$H_2O/6.5/O_2/0.4/N_2/1.0/$			
15	$O + H + M \rightarrow OH + M$	$1.00 \cdot 10^{16}$	0	0
	$O + H + M \leftarrow OH + M$	$7.94 \cdot 10^{19}$	-1.0	103 720
	$H_2O/6.5/O_2/0.4/N_2/1.0/$			
16	$O_2 + M \rightarrow 2O + M$	$5.13 \cdot 10^{15}$	0	115 000
	$O_2 + M \leftarrow 2O + M$	$4.68 \cdot 10^{15}$	-0.28	0
	$H_2O/6.5/O_2/0.4/N_2/1.0/$			
17	$H_2 + M \rightarrow 2H + M$	$2.19 \cdot 10^{14}$	0	96 000
	$H_2 + M \leftarrow 2H + M$	$3.02 \cdot 10^{15}$	0	0
	$H_2O/6.5/O_2/0.4/N_2/1.0/$			

Wilson–MacCormack Model

ELEMENTS
H O N
SPECIES
H O H_2 O_2 OH H_2O HO_2 H_2O_2 N_2

No.	Reaction	A, mol, cm^3, s	β	E_a, cal/mol
1	$H_2 + O_2 \leftrightarrow HO_2 + H$	$1.0 \cdot 10^{14}$	0	56 000
2	$H + O_2 \leftrightarrow OH + O$	$2.6 \cdot 10^{14}$	0	16 800
3	$O + H_2 \leftrightarrow OH + H$	$1.8 \cdot 10^{10}$	1.0	8900
4	$OH + H_2 \leftrightarrow H + H_2O$	$2.2 \cdot 10^{13}$	0	5150
5	$2OH \leftrightarrow O + H_2O$	$6.3 \cdot 10^{12}$	−2.0	1090
6	$H + OH + M \leftrightarrow H_2O + M$	$2.2 \cdot 10^{22}$	−1.0	0
	$H_2O/6.0/N_2/1.0/$			
7	$2H + M \leftrightarrow H_2 + M$	$6.4 \cdot 10^{17}$	−0.6	0
	$H_2/2.0/H_2O/6.0/N_2/1.0/$			
8	$H + O + M \leftrightarrow OH + M$	$6.0 \cdot 10^{16}$	0	0
	$H_2O/5.0/N_2/1.0/$			
9	$H + O_2 + M \leftrightarrow HO_2 + M$	$2.1 \cdot 10^{15}$	0	−1000
	$H_2/2.0/H_2O/16.0/N_2/1.0/$			
10	$2O + M \leftrightarrow O_2 + M$	$6.0 \cdot 10^{13}$	0	−1800
11	$HO_2 + H \leftrightarrow 2OH$	$1.4 \cdot 10^{14}$	0	1080
12	$HO_2 + H \leftrightarrow H_2O + O$	$1.0 \cdot 10^{13}$	0	1080
13	$HO_2 + O \leftrightarrow O_2 + OH$	$1.5 \cdot 10^{13}$	0	950
14	$HO_2 + OH \leftrightarrow H_2O + O_2$	$8.0 \cdot 10^{12}$	0	0
15	$2HO_2 \leftrightarrow H_2O_2 + O_2$	$2.0 \cdot 10^{12}$	0	0
16	$H + H_2O_2 \leftrightarrow H_2 + HO_2$	$1.4 \cdot 10^{12}$	0	3600
17	$O + H_2O_2 \leftrightarrow OH + HO_2$	$1.4 \cdot 10^{13}$	0	6400
18	$OH + H_2O_2 \leftrightarrow H_2O + HO_2$	$6.1 \cdot 10^{12}$	0	1430
19	$H_2O_2 + M \leftrightarrow 2OH + M$	$1.2 \cdot 10^{17}$	0	45 500
	$H_2O/15.0/N_2/1.0/$			

Petersen–Hanson Model

ELEMENTS
H O N
SPECIES
H O H_2 O_2 OH H_2O HO_2 H_2O_2 N_2

No.	Reaction	A, mol, cm^3, s	β	E_a, cal/mol
1	$O + H_2 \leftrightarrow H + OH$	$5.00 \cdot 10^{04}$	2.7	6290
2	$H + O_2 + M \leftrightarrow HO_2 + M$	$2.80 \cdot 10^{18}$	−0.9	0
	$O_2/0/H_2O/0/N_2/0/$			
3	$H + 2O_2 \leftrightarrow HO_2 + O_2$	$3.00 \cdot 10^{20}$	−1.7	0
4	$H + O_2 + H_2O \leftrightarrow HO_2 + H_2O$	$9.38 \cdot 10^{18}$	−0.8	0
5	$H + O_2 \leftrightarrow O + OH$	$8.30 \cdot 10^{13}$	0	14 413
6	$H + HO_2 \leftrightarrow O_2 + H_2$	$2.80 \cdot 10^{13}$	0	1068
7	$H + HO_2 \leftrightarrow 2OH$	$1.34 \cdot 10^{14}$	0	635
8	$H + H_2O_2 \leftrightarrow HO_2 + H_2$	$1.21 \cdot 10^{07}$	2.0	5200
9	$OH + H_2 \leftrightarrow H_2O + H$	$2.16 \cdot 10^{08}$	1.5	3430
10	$2OH(+ M) \leftrightarrow H_2O_2(+ M)$	$7.40 \cdot 10^{13}$	−0.4	0
	LOW / $2.30 \cdot 10^{18}$ −0.9 −1 700 / TROE / 0.7346, 94.0, 1 756.0, 5 182.0 / H_2/2.0/H_2O/6.0/N_2/1.0/			
11	$OH + HO_2 \leftrightarrow O_2 + H_2O$	$2.90 \cdot 10^{13}$	0	−500
12	$OH + H_2O_2 \leftrightarrow HO_2 + H_2O$	$1.75 \cdot 10^{12}$	0	320
13	$OH + H_2O_2 \leftrightarrow HO_2 + H_2O$	$5.80 \cdot 10^{14}$	0	9560
14	$2HO_2 \leftrightarrow O_2 + H_2O_2$	$1.30 \cdot 10^{11}$	0	−1630
15	$2HO_2 \leftrightarrow O_2 + H_2O_2$	$4.20 \cdot 10^{14}$	0	12 000
16	$2O + M \leftrightarrow O_2 + M$	$1.20 \cdot 10^{17}$	−1.0	0
	H_2/2.4/H_2O/15.4/N_2/1.0/			
17	$O + H + M \leftrightarrow OH + M$	$5.00 \cdot 10^{17}$	−1.0	0
	H_2/2.0/H_2O/6.0/N_2/1.0/			
18	$H + OH + M \leftrightarrow H_2O + M$	$2.20 \cdot 10^{22}$	−2.0	0
	H_2/0.73/H_2O/3.65/N_2/1.0/			
19	$2H + M \leftrightarrow H_2 + M$	$1.00 \cdot 10^{18}$	−1.0	0
	H_2/1.7/H_2O/7.0/N_2/1.0/			
20	$H + O_2 + N_2 \leftrightarrow HO_2 + N_2$	$2.60 \cdot 10^{19}$	−1.2	0

REFERENCES

1. V. P. Korobeinikov and V. A. Levin, "Strong Explosion in a Combustible Gas Mixture," Izv. Akad. Nauk SSSR, Mekh. Zhidk. Gaza, No. 6, 58–51 (1969).
2. Yu. A. Nikolaev and D. V. Zak, "Agreement of Models of Chemical Reactions in Gases with the Second Law of Thermodynamics," Fiz. Goreniya Vzryva **24** (4), 87–90 (1988) [Combust., Expl., Shock Waves **24** (4), 461–463 (1988)].
3. I. A. Bedarev and A. V. Fedorov, "Comparative Analysis of Three Mathematical Models of Hydrogen Ignition," Fiz. Goreniya Vzryva **42** (1), 26–33 (2006) [Combust., Expl., Shock Waves **42** (1), 19–26 (2006)].
4. I. A. Bedarev, K. V. Rylova, and A. V. Fedorov, "Application of Detailed and Reduced Kinetic Schemes for the Description of Detonation of Diluted Hydrogen–Air Mixtures," Fiz. Goreniya Vzryva **51** (5), 22–33 (2015) [Combust., Expl., Shock Waves **51** (5), 528–539 (2015)].
5. E. Hairer and G. Wanner, *Solving Ordinary Differential Equations II. Stiff and Differential–Algebraic Problems* (Springer-Verlag, Berlin–Heidelberg, 1996).
6. S. Browne, J. Ziegler, and J. E. Shepherd, "Numerical Solution Methods for Shock and Detonation Jump Conditions," GALCIT Report No. FM2006.006–R3 (California Inst. of Technology, 2018).
7. D. M. Davidenko, I. Gökalp, E. Dufour, and P. Magre, "Systematic Numerical Study of the Supersonic Combustion in an Experimental Combustion Chamber," in *14th AIAA/AHI Space Planes and Hypersonic Systems and Technologies Conference*, Paper No. 2006-7913 (2006) ; doi.org/10.2514/6.2006-7913.
8. R. Deiterding, "Parallel Adaptive Simulation of Multi-Dimensional Detonation Structures," Diss. Doktor der Naturwissenschaften, Technischen Universität Cottbus (Brandenburg, Germany, 2003).
9. C. K. Westbrook, "Chemical Kinetics of Hydrocarbon Oxidation in Gaseous Detonations," Combust. Flame **46**, 191–210 (1982); doi.org/10.1016/0010-2180(82)90015-3.
10. G. J. Wilson and R. W. MacCormack, "Modeling Supersonic Combustion using a Fully Implicit Mumerical Method," AIAA J. **30** (4), 1008–1015 (1992); doi.org/10.2514/3.11021.
11. C. J. Jachimowski, "An Analytical Study of the Hydrogen-Air Reaction Mechanism with Application to Scramjet Combustion," NASA TP 2791 (1988).
12. E. L. Petersen and R. K. Hanson, "Reduced Kinetics Mechanisms for Ram Accelerator Combustion," J. Propul. Power **15** (4), 591–600 (1999); doi.org/10.2514/2.5468.
13. A. Burcat, "Ideal Gas Thermodynamic Data in Polynomial Form for Combustion and Air Pollution Use," garfield.chem.elte.hu/Burcat/burcat.html.
14. S. P. Borisov, A. N. Kudryavtsev, and A. A. Shershnev, "Development and Validation of the Hybrid Code for Numerical Simulation of Detonations," J. Phys.: Conf. Ser. **1105**, 012037 (2018); DOI: 10.1088/1742-6596/1105/1/012037.
15. M. Short and D. S. Stewart, "Cellular Detonation Stability. Part 1. A Normal-Mode Linear Analysis," J. Fluid Mech. **368**, 229–262 (1998).
16. S. P. Borisov and S. P. Kudryavtsev, "Numerical Simulation of Nonlinear Dynamics of 1D Pulsating Detonations," J. Phys.: Conf. Ser. **894**, 012013 (2017); DOI: 10.1088/1742-6596/894/1/012013.
17. S. P. Borisov, A. N. Kudryavtsev, and A. A. Shershnev, "Influence of Detailed Mechanisms of Chemical Kinetics on Propagation and Stability of Detonation Wave in H_2/O_2 Mixture," J. Phys.: Conf. Ser. **1382**, 012052 (2019); DOI: 10.1088/1742-6596/1382/1/012052.
18. B. V. Voitsekhovskii, V. V. Mitrofanov, and M. E. Topchiyan, *Structure of the Detonation Front in Gases* (Izd. Sib. Otd. Akad. Nauk SSSR, Novosibirsk, 1963) [in Russian].
19. W. Ficket and W. C. Davis, *Detonation* (Univ. of California Press, Berkeley, 1979).
20. G. J. Sharpe and J. J. Quirk, "Nonlinear Cellular Dynamics of the Idealized Detonation Model: Regular Cells," Combust. Theory Model. **12** (1), 1–21 (2008); doi.org/10.1080/13647830701335749.
21. S. P. Borisov and A. N. Kudryavtsev, "Linear and Nonlinear Effects in Detonation Wave Structure Formation," J. Phys.: Conf. Ser. **722**, 012022 (2016); DOI: 10.1088/1742-6596/722/1/012022.
22. A. N. Kudryavtsev and S. P. Borisov, "Stability of Detonation Waves Propagating in Plane and Rectangular Channels," Fiz. Goreniya Vzryva **56** (1), 105–113 (2020) [Combust., Expl., Shock Waves **56** (1), 92–99 (2020); DOI: 10.1134/S0010508220010116].
23. R. A. Strehlow, "Transverse Waves in Detonations: II. Structure and Spacing in H_2–O_2, C_2H_2–O_2, C_2H_4–O_2 and CH_4–O_2 Systems," AIAA J. **7** (3), 492–496 (1969).
24. M. J. Kaneshige, "Gaseous Detonation Initiation and Stabilization by Hypervelocity Projectiles," Ph. D. Thesis (California Inst. of Technology, Pasadena, 1999).
25. S. Yungster and K. Radhakrishnan, "Pulsating One-Dimensional Detonations in Hydrogen–Air Mixtures," Combust. Theory Model. **8** (4), 745–770 (2004); doi.org/10.1088/1364-7830/8/4/005.
26. Y. Daimon and A. Matsuo, "Unsteady Features on One-Dimensional Hydrogen-Air Detonations," Phys. Fluids **19** (11), 116101 (2007); doi.org/10.1063/1.2801478.
27. L. K. Cole, A. R. Karagozian, and J.-L. Cambier, "Stability of Flame-Shock Coupling in Detonation Waves: 1D Dynamics," Combust. Sci. Technol. **184** (10/11), 1502–1525 (2011); DOI: 10.1080/00102202.2012.690316.